Hydride Formation in Zirconium Alloys

Arthur T. Motta & Long-Qing Chen

JOM
The Journal of The Minerals, Metals &
Materials Society (TMS)

ISSN 1047-4838
Volume 64
Number 12

JOM (2012) 64:1403-1408
DOI 10.1007/s11837-012-0479-x

JOM
An official publication of The Minerals, Metals & Materials Society
TMS2013: Where Materials Science Meets Industrial Application
DECEMBER 2012
jom.tms.org
TMS
Springer
HIGH-TEMPERATURE MATERIALS
■ Light Water Reactor Fuels
■ Gas-Alloy Interactions at Elevated Temperatures
■ Corrosion at High Temperatures

Springer

Your article is protected by copyright and all rights are held exclusively by TMS. This e-offprint is for personal use only and shall not be self-archived in electronic repositories. If you wish to self-archive your work, please use the accepted author's version for posting to your own website or your institution's repository. You may further deposit the accepted author's version on a funder's repository at a funder's request, provided it is not made publicly available until 12 months after publication.

Springer

JOM, Vol. 64, No. 12, 2012
DOI: 10.1007/s11837-012-0479-x
© 2012 TMS

Hydride Formation in Zirconium Alloys

ARTHUR T. MOTTA[1,3] and LONG-QING CHEN[2]

1.—Department of Mechanical and Nuclear Engineering, The Pennsylvania State University, University Park, PA 16802, USA. 2.—Department of Materials Science and Engineering and the Materials Research Institute, The Pennsylvania State University, University Park, PA 16802, USA. 3.—e-mail: atm2@psu.edu

The ingress of hydrogen during corrosion in service can degrade the mechanical properties of zirconium alloy nuclear fuel cladding because of the formation of brittle hydrides. The formation of these hydrides is reviewed in light of recent synchrotron radiation experimental results and phase-field modeling computational results that provide new insight on the process.

INTRODUCTION

In the nuclear reactor environment, both the fuel and the fuel cladding evolve under the influence of various driving forces such as temperature, radiation damage, fission product creation, stress, corrosive environment, etc.[1] In light-water reactors, there is considerable experience on the behavior of zirconium alloy nuclear fuel cladding up to burnup levels of up to 30–35 GWd/ton and corresponding exposures. However, driven by the need to minimize waste volume, increase capacity factors, and reduce fuel costs, the industry has increased the average discharge fuel burnup with a consequent increase in exposure time.[2] Such increases take the fuel into an operation regime in which fuel degradation mechanisms are less well understood. In addition to increased radiation damage (the number of displacements per atom (DPA) increases roughly in proportion to the reactor exposure), increased corrosion of the fuel cladding can occur, with a concomitant increase in hydrogen ingress. This increased corrosion is caused not only by increased exposure but also by the fact that the primary water chemistry is more aggressive, due to the additions necessary to operate at higher burnup. Finally, utilities are proposing or have received licenses for power uprates in many reactors. Power uprates allow utilities to squeeze some additional power out of existing units, which causes increases in the outlet temperature and some boiling to occur in the core of pressurized water reactors. Thus, the fuel operates at a higher temperature with increased radiation damage and under more aggressive chemistry. All of these factors combine to significantly increase the duty[3] on the fuel cladding (higher radiation damage, increased corrosion and hydriding, CRUD deposition, etc.), and it is necessary to show that fuel failures will not increase as a result.[4]

By fuel failures, it is meant *cladding* failures. As a result, the proposed more severe duty cycles require greater resistance of the cladding to failure, especially in view of the industry's stated goals of zero fuel failures.[2] Some of the principal mechanisms of failure during longer reactor exposures are related to hydrogen ingress during corrosion, associated with the formation of brittle hydrides and concomitant degradation of mechanical properties.[5] In this article, we discuss the formation of hydrides within the fuel cladding during reactor exposure and the influence of particular hydride microstructures on cladding ductility.

HYDRIDE FORMATION

The hydrogen entering the cladding remains in solid solution until the solubility limit is reached. The terminal solid solubility of hydrogen in Zircaloy $C^{\mathrm{H}}_{\alpha-\mathrm{Zr}}$ has previously been measured and is given by

$$C^{\mathrm{H}}_{\alpha-\mathrm{Zr}} = A\exp(-E_{\mathrm{H}}/T)$$

where A is a constant, equal to 1.2×10^5 wt. ppm, and E_{H} is the is the difference in partial molar heat of solution of hydrogen in solid solution and partial molar heat of solution of hydrogen in hydrides. The numerical value of $E_{\mathrm{H}}/k_{\mathrm{B}}$ is 4,300 K.[6,7] At the reactor fuel cladding temperature (approximately 340°C at the outer tube diameter and 370°C to 380°C at the inner tube diameter), the hydrogen solubility is 100–150 wt. ppm. The hydrogen solubility in Zircaloy in the reactor environment can

(Published online October 23, 2012)

differ from the value above, as discussed by McMinn et al.[6]

The hydrogen terminal solid solubility (TSS) is different when measured in dissolution or in precipitation (TSS_d and TSS_p), that is, a hysteresis is observed that causes hydride dissolution to occur at a higher temperature than hydride precipitation.[8] Figure 1 shows the hydride dissolution and precipitation temperatures, as determined using in situ synchrotron radiation diffraction and compared to differential scanning calorimetry (DSC).[9]

Response to Thermal and Stress Gradients

Because hydrogen is quite mobile in Zr alloy cladding, the presence of temperature and stress gradients induces inhomogeneous hydride distributions. In general, because failure will occur in the weakest spot in the cladding, the *local* hydrogen content is more important than the *average* hydrogen content to determine failure. Therefore, an estimation of this variation is crucial to the assessment of fuel safety, both in the reactor and in dry storage.

Hydrogen tends to concentrate in the colder regions and in regions of high stress concentration. For example, it is well known that a hydride rim forms in Zr alloy cladding at high burnup. The explanation for the formation of such a rim is that the outer skin of the cladding tube is cooler, and thus, the hydrogen solubility limit is reached there first. Figure 2 shows a hydride rim formed during reactor exposure.

The concentration of hydrogen in specific spots can in fact occur in the three principal tube directions. In the *radial* direction, as mentioned above, the lower temperature in the cladding outer rim can cause hydride formation to occur there first. In the *axial* direction, increased corrosion in the upper grid spans causes the hydride concentration to increase with height. In addition, the interpellet region is colder, causing hydrogen to concentrate locally in that region. Although at first glance, symmetry considerations would preclude hydrogen accumulation in the *azimuthal* direction, studies have shown that the azimuthal concentration of hydrogen can vary considerably.[12,13] Examinations of the cladding material shown in Fig. 2 (from H.B. Robinson, 67 GWd/t) show an average hydrogen content of 600 wt. ppm but a variation of ±200 wt. ppm around the circumference. Also, the loss of oxide by spallation that can occur in high burnup fuel increases the local thermal conductivity, resulting in a cold spot where hydride blisters can form Ref. [14].

In addition to responding to thermal gradients normally present during reactor operation, hydrogen can respond to stress concentrations such as a crack tip. The elevated stress is thought to effectively decrease the hydrogen solubility near the crack tip causing preferential hydride precipitation. The hydride precipitate can then advance, creating a new stress concentration, and the process repeats.[15] This is the phenomenon of delayed hydride cracking (DHC), which is of greater concern in the Canadian heavy water reactors, but can occur in some light water reactors as well.[8,16–20]

Hydride Precipitation

The stable hydride phase at low temperature is the delta hydride phase, which is in fact the phase normally observed experimentally,[21,22] although the gamma phase can be observed at high hydrogen contents.[23] Hydrides normally precipitate as platelets whose normals are parallel to the radial direction. The orientation relationship of $0001_{hcpZr}//111_{delta}$ has been discerned.[21] The macroscopic hydrides are said to be composed of several smaller

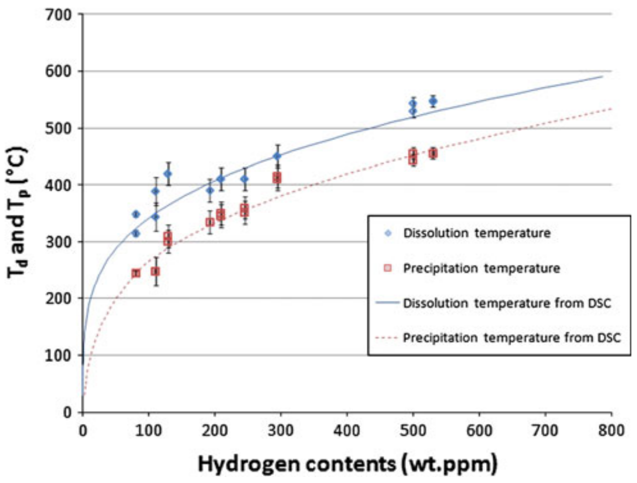

Fig. 1. Hydrogen dissolution and precipitation temperatures as determined using in situ synchrotron radiation diffraction and compared to DSC results.[9,10]

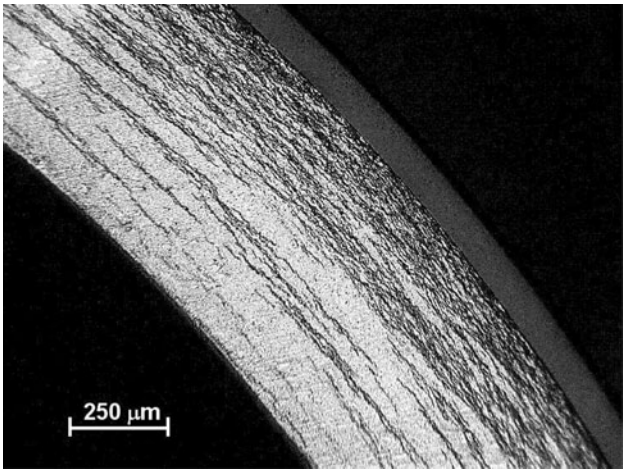

Fig. 2. Cross section optical micrograph of Zircaloy-4 alloy cladding in high-burnup PWR fuel (H.B. Robinson, 67 GWd/t, containing 600 wt. ppm H), showing a rim of hydride precipitates near the outer surface (photo courtesy M. Billone, Argonne National Laboratory).[11]

stacked hydrides aligned with the overall orientation of approximately $[10\bar{1}7]$,[24,25] and they have some preference for nucleation at the alpha grain boundaries.

The Zr-H binary phase diagram[26] contains several metastable and stable hydride phases including the stable face-centered cubic (fcc) δ phase, the metastable face-centered tetragonal (fct) γ phase ($c/a > 1$), and the fct ε phase ($c/a < 1$). As Zr alloys pick up hydrogen in service, hydrides start to nucleate and grow when the hydrogen concentration reaches its solubility limit in the alloy. At the same time, the formation of hydrides leads to anisotropic elastic and plastic deformations. The interfacial energy between hydrides and Zr matrix tends to be highly anisotropic due to the mixed coherency of the interfaces, i.e., the habit plane is coherent and the edge plane is semicoherent or incoherent. The estimated interfacial energies are $\gamma_{\text{habit}} \sim 0.065$ and $\gamma_{\text{edge}} = 0.28$ (in J/m^2).[27] As a result, different thermomechanical loading conditions can produce quite different hydride precipitate microstructures. The morphology and spatial distribution of hydrides are crucial for understanding the fracture initiation and, thus, for improving the long-term stability of Zr-alloys against failure.

Conventional theoretical treatment of hydride precipitation in Zr alloys typically uses simplifying assumptions. For example, the diffusion of hydrogen atoms under the influence of a stress gradient is usually described by the conventional diffusion equation while ignoring the elastic and chemical interactions among hydrogen atoms. Often, only a single hydride is allowed to grow, and hence, hydride–hydride interactions are not considered. Isotropic elasticity is usually assumed for determining stress distributions, and the polycrystalline nature of the alloy is ignored.

A powerful method for modeling hydride microstructure evolution is the phase-field method.[28–30] In a phase-field model, an inhomogeneous microstructure (i.e., hydrides embedded in a polycrystalline Zr matrix) is described by a set of field variables that represent the local hydrogen concentration, orientational variant distributions and morphology of hydrides, and the grain orientations of the polycrystalline Zr matrix. The total free energy of such an inhomogeneous microstructure includes contributions from local bulk chemical free energy density, interfacial energies, and strain energy. The temporal evolution of the hydrogen concentration field is obtained by solving the Cahn–Hilliard equation[31] and that of the nonconserved order parameters describing the hydride variant and Zr-matrix grain orientation distributions by the Allen–Cahn equation.[32] With the phase-field method, it is possible to obtain the temporal and spatial evolution of hydrides during precipitation under both uniform and nonuniform applied stress as well as plastic deformation. The model automatically takes into account the interactions among hydride particles. The inhomogeneous elasticity can be efficiently taken into account for polycrystalline materials within the phase-field model.[33] The nucleation process can be introduced by either the Langevin noise method[34] or the explicit nucleation method using either sharp-interface critical nuclei[35] or using diffuse-interface critical nuclei.[36]

The phase-field method has been applied to the modeling of the morphology of γ-hydride formation in Zr-alloys.[34,37–42] The γ-hydrides are experimentally observed to be platelets parallel to the $\{10\bar{1}0\}$ planes of the matrix. On the (0001) plane of hexagonal zirconium matrix, they appear needle-like with axis along the three $\langle 11\bar{2}0\rangle$ directions. Due to the significant structural difference between the hydrides and Zr matrix, elastic strain energy plays a dominant role in determining the hydride morphology. Without external load, all three equivalent variants appear with the same probability during the nucleation process and grow along habit plains with an angle about 120 deg between each other. Figure 3a shows an example of morphology and spatial distribution of γ-hydrides obtained from a phase-field simulation.[34] Different variants arrange in such a way that the strain energy caused by the variant is minimized. However, if an external strain or stress is applied during a precipitation process, then hydrides tend to align perpendicular to the direction of the applied tensile load, as shown in Fig. 3b. The stress effect and variant alignment are most evident during the initial nucleation stage. As expected, the hydride density is higher at grain boundaries than in the corresponding bulk. Introduction of an inhomogeneous stress field due to a structural defect, e.g., a notch, produces higher density of hydride precipitates at the notch tip area. It is shown that the hydrides appear in the direction perpendicular to the notch surface at the notch boundary, and the hydrides in the area away from the notch tip arrange in a circular-like shape. The morphology pattern obtained from the simulation is qualitatively in agreement with the experimental observation. However, a significant difference between simulation results and experimental observation exists presumably because the plastic

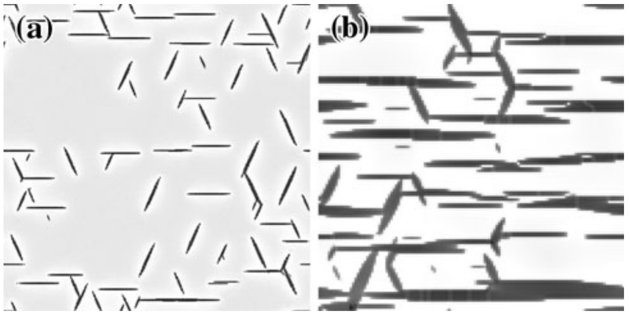

Fig. 3. (a) Morphology and distribution of γ-hydrides along the basal plane of Zr matrix. (b) Variant orientation of γ-hydrides under an applied stress/strain.[34]

deformation around the notch area was ignored in the simulation. To take into account the effect of plasticity, an elastoplastic phase-field model was developed to simulate the morphology evolution of hydride precipitation in zirconium bulk material with or without flaws. It is shown that the plastic deformation significantly decreases the stress level around hydrides. In addition, an externally applied stress not only leads to stress reorientation of hydride precipitates but also may result in crack initiation at the hydrides.[34]

The most commonly observed hydride in Zr alloys exhibits the δ crystal structure. According to the phase diagram, the equilibrium compositions at room temperature are approximately $X_\alpha \sim 0.08$ and $X_\delta \sim 0.58$.[26] Its formation involves a structural transformation from the hexagonally close packed (hcp) (α-phase) to the fcc (δ-phase) with a large volume expansion ($\sim$16%), leading to a plate-like shape for δ precipitates embedded in the Zr-alloy matrix (the lattice parameters of α and δ phases are $a_\alpha = 3.23$, $c_\alpha = 5.15$, $a_\delta = 4.77$ [in angstroms[43]). The stress-free transformation strain can be obtained by (I) shearing of the hcp lattice to change the (0001) plane stacking sequence, (II) lattice distortion along the basal plane, and (III) lattice expansion along the c-axis. The orientation relationship between α-Zr and δ-ZrH$_x$ is $(111)_\delta//(0001)_\alpha$or $[1\bar{1}0]_\delta//[11\bar{2}0]_\alpha$.[44] Heo et al.[45] recently conducted phase-field simulations of δ-hydride formation in both single-crystal and polycrystal zirconium.[45] The simulations accurately predicted the multivariant nature of δ-hydride plates in a Zr matrix. The habit planes of both individual variants and the multivariant plates obtained in the simulations agree with the existing experimental observation of the orientation relationship between α-Zr and δ-ZrH$_x$.[44] Phase-field simulations of δ-hydride reorientation under an applied stress are currently underway, and the results are being compared with in situ synchrotron measurements.[9]

EFFECT OF HYDRIDE CONCENTRATION AND DISTRIBUTION ON CLADDING DUCTILITY

The precipitation of these hydrides has significant impact on cladding ductility and failure[46–48] but not much impact on mechanical deformation.[49] In particular, the hydrides affect the resistance of the cladding to failure during a postulated reactivity-initiated accident (RIA),[50–51] which is one of the more challenging events for cladding survivability. An RIA may be caused by a control rod ejection or drop, inducing a near-instantaneous increase in reactivity in the nearby fuel rods. As a result of this reactivity insertion, the fission rate increases exponentially until the effect of Doppler broadening stops the chain reaction. The energy deposited in the fuel during the reactivity excursion causes the temperature of the fuel to increase, which in turn causes the fuel to expand and impinge on the cladding. Because this excursion occurs very fast, the cladding may remain close to its nominal operating temperature when the fuel impacts it. If the cladding has become embrittled from hydrogen ingress during reactor operation, then it can fail during such a transient. The possibility of such an accident has been recognized previously, and tests were conducted to establish the enthalpy limits to avoid fuel failure during a RIA.[53] Recent research showed that such limits may be degraded by long-term exposure of the fuel cladding to the reactor environment, causing radiation damage and hydriding.[54] As a result, significant work has been performed to reassess RIA limits at high fuel burnup.[55–67] Figure 4 shows the strain to failure determined during plane-strain testing of hydrided Zircaloy-4 containing a hydride rim as a function of hydride rim depth, for both room temperature and 300°C.[68] It is clear that material ductility is severely decreased beyond a hydride rim depth of about 100 μm.

In these cases, both the stress state and the loading path are crucial for determining cladding ductility, and appropriate tests have to be devised for these conditions.[5] It is clear, however, that increases in hydride concentration severely decrease ductility,[46,69] especially when these hydrides are concentrated in the form of hydride rims or blisters and deformed under a multiaxial state of stress.[68–70] Several of these studies[69,71] have shown different failure mechanisms at room and high temperature. Further research in this area is ongoing to determine the exact influence of hydrides on failure in each case. The use of synchrotron radiation to study deformation and failure in situ is a promising technique that can yield unique data of the strain partitioning between matrix and hydride and discern the deformation and failure mechanisms.[72]

Finally, the issue of hydride reorientation during dry storage and its impact on cladding ductility

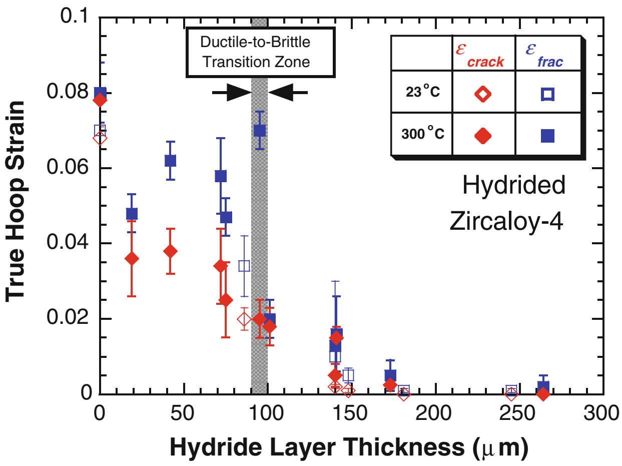

Fig. 4. Strain to failure during testing of hydrided Zircaloy-4.[7]

needs to be considered.[73,74] The drying operations involved in preparing the material for dry storage include heating the fuel rods to about 400°C for several cycles.[75,76] The imposed hoop stress from the fill gas on the cladding as it cools causes the hydrogen from the hydrides platelets that were dissolved during the drying operations to precipitate in the radial direction perpendicularly to the applied stress.[77] This can severely reduce cladding ductility during a postulated drop or handling accident.[74] Research is ongoing to determine the exact conditions (load, temperature history, and hydride concentration) that lead to a greater radial hydride fraction and greater embrittlement.[78]

CONCLUSIONS

Although extensive work has been performed to understand hydride behavior in zirconium alloys, much remains to be understood. This is for the most part because of the complexity of the phenomena involving coupling among chemistry, thermodynamics, stresses, and hydrogen diffusion. The recent use of state-of-the-art experimental procedures, especially involving in situ measurements, and the phase-field computational technique promises to address some of the fundamental questions in this field, especially when applied in tandem.

ACKNOWLEDGEMENTS

The authors would like to acknowledge discussions with Kimberly Colas, who was primarily responsible for much of the experimental work shown in this study, and with Taewook Heo, S. Q. Shi, and X. Q. Ma on phase-field simulations of hydride precipitation. The work was partially supported by grants number DMR-0710483 and DMR-0710616 from the National Science Foundation. Usage of the Advanced Photon Source was supported by the U.S. Department of Energy, Office of Basic Energy Sciences under Contract No. DE-AC02-06CH11357.

REFERENCES

1. C. Lemaignan and A.T. Motta, *Materials Science and Technology, A Comprehensive Treatment*, vol. 10 B, ed. B.R.T. Frost (New York: VCH, 1994), p. 1.
2. R. Yang, O. Ozer, and H. Rosenbaum, *Light Water Reactor Fuel Performance Meeting,* ed. P. Macdonald (Park City, UT: ANS, 2000).
3. G.P. Sabol, R. Comstock, G. Schoenberger, H. Kunishi, and D.L. Nuhfer, *Proceedings of International Topical Meeting on Light Water Reactor Fuel Performance*, Portland, OR (1997), p. 397.
4. A.T. Motta (Paper presented at Materials Research Society Fall Meeting, Symposium T: Materials Innovations for Next-Generation Nuclear Energy, Boston, MA, 2007).
5. J. Desquines, D.A. Koss, A.T. Motta, B. Cazalis, and M. Petit, *J. Nucl. Mater.* 412, 250 (2011).
6. A. McMinn, E.C. Darby, and J.S. Schofield, *12th Int. Symp. on Zr in the Nuclear Industry*, vol. STP-1354, ed. G.P. Sabol and J. Moan (Toronto, CA: ASTM, 2000), p. 173.
7. J.J. Kearns, *J. Nucl. Mater.* 22, 292 (1967).
8. M.P. Puls, *Acta Metall.* 29, 1961 (1981).
9. K.B. Colas, A.T. Motta, J.D. Almer, M.R. Daymond, M. Kerr, A.D. Banchik, P. Vizcaino, and J.R. Santisteban, *Acta Mater.* 58, 6575 (2010).
10. K. Une and S. Ishimoto, *J. Nucl. Mater.* 322, 66 (2003).
11. M. Billone, Y. Yan, T. Burtseva, and R. Daum, Cladding Embrittlement During Postulated Loss-of-Coolant Accidents, NRC, Doc.No NUREG/CR-6967 (2008).
12. D.D. Lanning, C.E. Beyer, and C.L. Painter, U.S. Nuclear Regulatory Commission NUREG CR-6534 (1997).
13. M.C. Billone, Y. Yan, T. Burtseva, and R.S. Daum, NRC, 2008.
14. A.M. Garde, G.P. Smith, R.C. Pirek, *11th International Symposium on Zr in the Nuclear Industry*, vol. STP 1295, ed. G.P. Sabol ERBa (Garmisch-Partenkirchen, Germany: ASTM, 1996), p. 407.
15. M.P. Puls, *Metall. Trans. A* 22A, 2327 (1991).
16. A. Sawatzky and C.E. Ells, *12th ASTM International Symposium on Zirconium in the Nuclear Industry*, Toronto, Canada, STP 1354 (2000), p. 32.
17. B.A. Cheadle, C.E. Coleman, and J.F. Ambler, *7th International Symposium on Zr in the Nuclear Industry*, vol. STP-939 (Philadelphia, PA: ASTM, 1987), p. 224.
18. M.P. Puls, *Metall. Trans. A* 19A, 2247 (1988).
19. L.A. Simpson and C.D. Cann, *J. Nucl. Mater.* 87, 303 (1979).
20. L.A. Simpson and M.P. Puls, *Metall. Trans. A* 10A, 1093 (1979).
21. D.L. Douglass, *The Metallurgy of Zirconium*. (Vienna: International Atomic Energy Agency Supplement, 1971).
22. C.E. Ells, *J. Nucl. Mater.* 28, 129 (1968).
23. R.S. Daum, Y.S. Chu, and A.T. Motta, *J. Nucl. Mater.* 392, 453 (2009).
24. A. Racine (Ph.D. thesis, L'Ecole Polytechnique, 2005).
25. H.M. Chung, R.S. Daum, J.M. Hiller, and M.C. Billone, 13th International Symposium on Zirconium in the Nuclear Industry, Annecy, France, ASTM STP 1423 (2002), p. 561.
26. G.G. Libowitz, *J. Nucl. Mater.* 5, 228 (1962).
27. A.R. Massih and L.O. Jernkvist, *Comp. Mater. Sci.* 46, 1091 (2009).
28. L.-Q. Chen Annu, *Rev. Mater. Res.* 32, 113 (2001).
29. H. Emmerich, *Adv. Phys.* 57, 1 (2008).
30. I. Steinbach, *Mater. Sci. Eng.* 17, 073001 (2009).
31. J.W. Cahn and J.E. Hilliard, *J. Chem. Phys.* 28, 258 (1958).
32. S.M. Allen and J.W. Cahn, *J. Phys.* C7 (1977).
33. S. Bhattacharyya, T.W. Heo, K. Chang, and L.-Q. Chen, *Model. Simul. Mater. Sci. Eng.* 19, 035002 (2011).
34. X.Q. Ma, S.Q. Shi, C.H. Woo, and L.-Q. Chen, *Comp. Mater. Sci.* 23, 283 (2002).
35. Y.H. Wen, J.P. Simmons, C. Shen, C. Woodward, Y. Wang, *Acta Mater.* 51, 1123 (2003).
36. T.W. Heo, L. Zhang, Q. Du, and L.-Q. Chen, *Scripta Mater.* 63, 8 (2010).
37. X.H. Guo, S.Q. Shi, Q.M. Zhang, and X.Q. Ma, *J. Nucl. Mater.* 378, 120 (2008).
38. X.H. Guo, S.Q. Shi, Q.M. Zhang, and X.Q. Ma, *J. Nucl. Mater.* 378, 110 (2008).
39. Y.H. He, X.H. Guo, and Q.M. Zhang, *Int. J. Nonlin. Sci. Numer. Simulat.* 9, 103 (2008).
40. X.Q. Ma, S.Q. Shi, S.Y. Hu, C.H. Woo, and L.-Q. Chen, *J. Univ. Sci. Technol. Beijing* 12, 416 (2005).
41. X.Q. Ma, S.Q. Shi, C.H. Woo, and L.-Q. Chen, *Mater. Sci. Eng., A* 334, 6 (2002).
42. X.Q. Ma, S.Q. Shi, C.H. Woo, and L.-Q. Chen, *Scripta Mater.* 47, 237 (2002).
43. Y. Udagawa, M. Yamaguchi, H. Abe, N. Sekimura, and T. Fuketa, *Acta Mater.* 58, 3927 (2010).
44. D.O. Northwood and R.W. Gilbert, *J. Nucl. Mater.* 78, 112 (1978).
45. T.W. Heo, K.B. Colas, A.T. Motta, and L.-Q. Chen, unpublished (2011).
46. S. Arsene, J. Bai, and P. Bompard, *Metall. Mater. Trans. A* 34A, 579 (2003).
47. J.B. Bai, N. Ji, D. Gilbon, C. Prioul, and D. Francois, *Metall. Mater. Trans. A* 25A, 1199 (1994).
48. J.B. Bai, C. Prioul, and D. Francois, *Metall. Mater. Trans. A* 25A, 1185 (1994).

49. M.E. Flanagan, D.A. Koss, and A.T. Motta, *Proceedings of the 2008 Water Reactor Fuel Performance Meeting*, Seoul, Korea (2008).
50. B.E. Boyack, A.T. Motta, K.L. Peddicord, C.A. Alexander, R.C. Deveney, B.M. Dunn, T. Fuketa, K.E. Higar, L.E. Hochreiter, S.E. Jensen, F.J .Moody, M.E. Nissley, J. Papin, G. Potts, D.W. Pruitt, J. Rashid, D.H. Risher, R.J. Rohrer, J.S. Tulenko, K. Valtonen, and W. Wiesenack, Phenomena Identification and Ranking Tables (PIRTs) for Reactivity Initiated Accidents in Pressurized Water Reactors Containing High Burnup Fuel, Nuclear Regulatory Commission, NUREG/CR-6742 (2001).
51. R. Meyer, R.K. McCardell, and H.H. Scott, *International Topical Meeting on Light Water Reactor Fuel Performance* (Portland, OR: American Nuclear Society, 1997), p. 729.
52. R.O. Meyer, *Nucl. Technol.* 155, 293 (2006).
53. P.E. MacDonald, S.L. Seiffert, Z.R. Martinson, R.K. McCardell, D.E. Owen, and S.K. Fukuda, *Nucl. Safety* 21, 582 (1980).
54. R.O. Meyer, R.K. McCardell, H.M. Chung, D.J. Diamond, and H.H. Scott, *Nucl. Safety* 37, 372 (1996).
55. R.S. Daum, S. Majumdar, H. Tsai, T.S. Bray, D.A. Koss, A.T. Motta, and M.C. Billone, *Proc. 4th Int. Sym. on Small Specimen Test Techniques*, vol. STP 1418, ed. M.A. Sokolov, J.D. Landes, and G.E. Lucas (West Conshohocken, PA: ASTM, 2002), p. 195.
56. J. Papin, M. Balourdet, F. Lemoine, F. Lamare, J.M. Frizonnet, and F. Schmitz, *Nucl. Safety* 37, 289 (1996).
57. V. Asmolov and L. Yegorova, *Nucl. Safety* 37, 343 (1996).
58. F. Schmitz and J. Papin, *J. Nucl. Mater.* 270, 55 (1999).
59. R.S. Daum, S. Majumdar, D.W. Bates, A.T. Motta, D.A. Koss, and M.C. Billone, *13th International Symposium on Zirconium in the Nuclear Industry*, Annecy, France, ASTM STP 1423 (2002), p. 702.
60. R. Montgomery, N. Waeckel, and R. Yang, Topical Report on Reactivity Initiated Accidents: Bases for RIA Fuel and Core Coolability, Palo Alto, CA, EPRI Report Number 1002865, (2002).
61. R.O. Montgomery, Y.R. Rashid, O. Ozer, and R.L. Yang, *Nucl. Safety* 37, 372 (1996).
62. V. Grigoriev, R. Jakobsson, and D. Schrire, *24th NSRR Technical Review Meeting* (JAERI-Conf 2001-010) (Ibaraki-ken, Japan: JAERI, 2001), p. 139.
63. J. Desquines, B. Cazalis, C. Bernaudat, C. Poussard, X. Averty, P. Yvon, R. Daum, J. Rashid, and D. Schrire, *14th International Symposium on Zr in the Nuclear Industry*, vol. STP 1467 (Stockholm, Sweden: American Society for Testing and Materials (ASTM), 2005), p. 851.
64. B. Cazalis, J. Desquines, C. Poussard, M. Petit, Y. Monerie, C. Bernaudat, P. Yvon, and X. Averty, *Nucl. Technol.* 157, 215 (2007).
65. J. Papin, B. Cazalis, J.M. Frizonnet, J. Desquines, F. Lemoine, V. Georgenthum, F. Lamare, and M. Petit, *Nucl. Technol.* 157, 230 (2007).
66. T. Nakamura, T. Fuketa, T. Sugiyama, and H. Sasajima, *J. Nucl. Sci. Technol.* 41, 37 (2004).
67. F. Nagase and T. Fuketa, *J. Nucl. Sci. Technol.* 42, 58 (2005).
68. R.S. Daum, D.W. Bates, D.A. Koss, and A.T. Motta, *Proceedings of the International Conference on Hydrogen Effects on Material Behaviour and Corrosion Deformation Interactions, Sept 22–26 2002*, Moran, WY (Warrendale, PA: Minerals, Metals and Materials Society, 2003), p. 249.
69. A. Glendening, D.A. Koss, A.T. Motta, O.N. Pierron, and R.S. Daum, *J. ASTM Int.* 2, 1 (2005).
70. O.N. Pierron, D.A. Koss, A.T. Motta, and K.S. Chan, *J. Nucl. Mater.* 322, 21 (2003).
71. T.M. Link, D.A. Koss, and A.T. Motta, *Nucl. Eng. Design* 186, 379 (1998).
72. M. Kerr, M.R. Daymond, R.A. Holt, and J.D. Almer, *J. Nucl. Mater.* 380, 70 (2008).
73. R.S. Daum, S. Majumdar, and M.C. Billone, *2003 Nuclear Safety Research Conference* (Washington, DC: U.S. Nuclear Regulatory Commission, 2003), p. 85.
74. M. Aomi, T. Baba, T. Miyashita, K. Kamimura, T. Yasuda, Y. Shinohara, and T. Takeda, *J. ASTM Int.* 5 (2008), Paper ID JAI101262.
75. R.E. Einziger, (Lemont, IL: Argonne National Laboratory, 1998).
76. R.E. Einziger, Extending dry storage of spent LWR fuel for 100 years, Argonne National Lab., Doc.No ANL/CMT/CP-96494 (1998).
77. J.J. Kearns, *J. Nucl. Mater.* 27, 64 (1968).
78. K. Colas, A. Motta, M.R. Daymond, M. Kerr, and J. Almer, *J. ASTM Int.* 8 (2010), Paper ID JAI103033.